Received 17 June 2022; revised 22 July 2022 and 10 August 2022; accepted 27 August 2022. Date of publication 31 August 2022; date of current version 15 September 2022. The review of this article was arranged by Editor P.-W. Li.

Digital Object Identifier 10.1109/JEDS.2022.3203364

Multilayer Crossbar Array of Amorphous Metal-Oxide Semiconductor Thin Films for Neuromorphic Systems

ETSUKO IWAGI[1], TAKUMI TSUNO[2,3], TAKAHITO IMAI[2], YASUHIKO NAKASHIMA[3] (Senior Member, IEEE), AND MUTSUMI KIMURA[2,3] (Senior Member, IEEE)

1 Department of Electronics and Informatics, Ryukoku University, Otsu 5202194, Japan
2 Faculty of Advanced Science and Technology, Ryukoku University, Otsu 5202194, Japan
3 Graduate School of Science and Technology, Nara Institute of Science and Technology, Ikoma 6300192, Japan

CORRESPONDING AUTHOR: M. KIMURA (e-mail: mutsu@rins.ryukoku.ac.jp)

This work was supported in part by KAKENHI under Grant (C) 19K11876 and Grant (A) 22H00515; in part by the Artificial Intelligence Research Promotion Foundation; in part by KDDI Foundation; in part by the High-Tech Research Center in Ryukoku University; in part by the Laboratory for Materials and Structures in Tokyo Institute of Technology; and in part by the Research Institute of Electrical Communication in Tohoku University.

ABSTRACT A multilayer crossbar array has been developed using amorphous metal-oxide semiconductor (AOS) thin films and implemented into a neuromorphic system. The multilayer structure can be realized, because the AOS thin films can be deposited by a simple sputtering method without heat treatment, which does not damage the underlying structures. First, Au thin films are deposited by vapor evaporation as electrodes, an amorphous In-Ga-Zn-O (α-IGZO) thin film is deposited by a sputtering method as a conductance change layer, these processes are repeated, and a multilayer crossbar array is completed, where each of the three conductance change layers is sandwiched between the electrodes. Next, the multilayer crossbar array is implemented into a neuromorphic system with modified Hebbian learning, which enables autonomous learning without control circuitry, and an associative memory function is confirmed, which guarantees the possibility of further advanced functions. These results lead to astronomical large-scale integration (LSI) of synaptic elements in neuromorphic systems in the future.

INDEX TERMS Multilayer, crossbar array, amorphous metal-oxide semiconductor (AOS), thin film, neuromorphic system.

I. INTRODUCTION

Artificial intelligences are becoming indispensable technologies as fundamental infrastructures in various societies, such as character and image recognition, information search and supply, language translation and captioning, expert system, automatic driving, autonomous brains, etc [1]–[3]. Neural networks serve as representative manners of artificial intelligences, which mimic operation principle of biological brains [4]–[8]. However, the traditional ones are redundant and intricate software to conveniently run high-spec Neumann-architecture computer hardware, which is not customized for neural networks, and the machine size is incredibly bulky and power dissipation is also unbelievably huge. Neuromorphic systems provide bioinspired systems from the device level and practical solutions that compose neural networks solely of customized hardware, whose advantages are self-organization, self-learning, parallel distributed computing, and fault tolerance, and the machine size can be compact and power consumption can be low [9]–[12]. However, the conventional ones are based on silicon device and circuit technologies, whose disadvantages are that they are digital circuits and have two-dimensional structure, which are completely dissimilar from biological brains. The digital circuit require more circuits than analog devices, and the two-dimensional structure of course has a limitation to high integration than the three-dimensional structure. Crossbar arrays of memristors are promising suggestion beyond the silicon technologies [13], [14]. On the other hand, amorphous metal-oxide semiconductor (AOS) thin films are being investigated for diverse applications [15]–[27] and proposed

This work is licensed under a Creative Commons Attribution 4.0 License. For more information, see https://creativecommons.org/licenses/by/4.0/

TABLE 1. Comparison of neuromorphic systems.

	Conventional Si device	Crossbar Memristor	
		Conventional other devices	Proposed AOS thin film
Maturity	O	Δ	×
Circuit	× Digital	O Analog	O Analog
Structure	× 2-D	× 2-D	O 3-D
Similarity to brain	×	Δ	O
Miniaturization	O	O	Δ
Potential	Δ	Δ	O

Bad × Δ O Good

also for neuromorphic systems [28]–[38], whose advantages are that they have analog characteristic [39] and can have three-dimensional structure [40].

In this study, a multilayer crossbar array has been developed using AOS thin films and implemented into a neuromorphic system. The multilayer structure can be realized as three-dimensional structure, because the AOS thin films can be deposited by a simple sputtering method without pre-, in-situ-, and post-heat treatment, which does not damage the underlying structures. In this paper, first, the device structure and fabrication processes of the multilayer crossbar array will be explained. Next, the multilayer crossbar array will be implemented into a neuromorphic system with modified Hebbian learning [41], and a neuromorphic function will be confirmed. These results will lead to the feasibility of astronomical large-scale integration (LSI) of synaptic elements in neuromorphic systems in the future.

II. MULTILAYER CROSSBAR ARRAY OF AMORPHOUS METAL-OXIDE SEMICONDUCTOR THIN FILMS

The multilayer crossbar array of AOS thin films is shown in Fig. 1. The cross-sectional illustration is shown in Fig. 1(a), and the overview photograph is shown in Fig. 1(b). The device structure is extremely simple, where each of the three conductance change layers is sandwiched between the electrodes. The fabrication processes are as follows. First, a quartz glass substrate is prepared, whose thickness is 0.7 mm and size is 3 × 3 cm. Next, a Au thin film is deposited by vapor evaporation, whose thickness is 80 nm, and patterned through a metal mask, whose line and space widths are 1.2 and 1.2 mm and number of lines is 10, as the first electrodes. Sequentially, an amorphous In-Ga-Zn-O (α-IGZO) thin film is deposited by radio-frequency (RF) magnetron sputtering method with a ceramic target of In:Ga:Zn=1:1:1, sputtering gas of Ar:O_2=5:15, deposition pressure of 2 Pa, and plasma power of 60 W, at room temperature, whose thickness is 90 nm, as the lower conductance change layer. Then, a Au thin film is again deposited through the metal mask, which is placed orthogonal to the first electrodes, as the second electrodes. Repeatedly, the α-IGZO and Au thin films are deposited two more times, as the middle conductance change layer, third electrodes, upper conductance change layer, and fourth electrodes. Finally, a multilayer crossbar array of AOS thin films

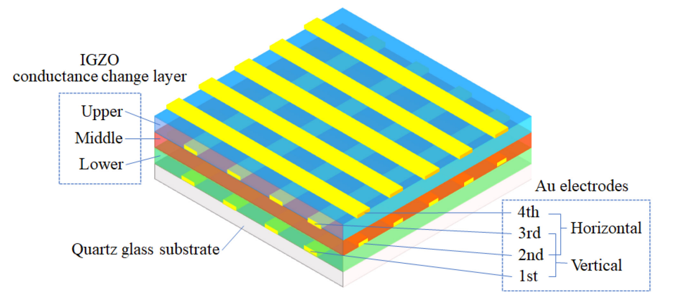

(a) Cross-sectional illustration.

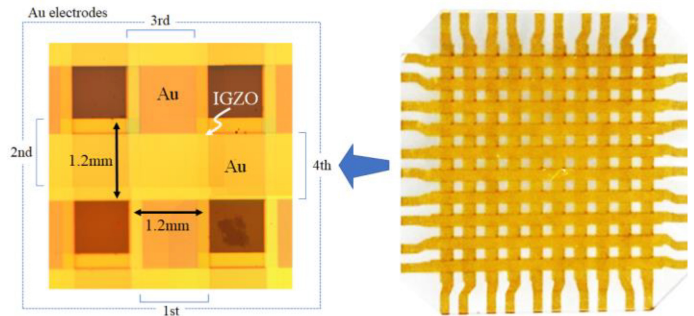

(b) Overview photograph.

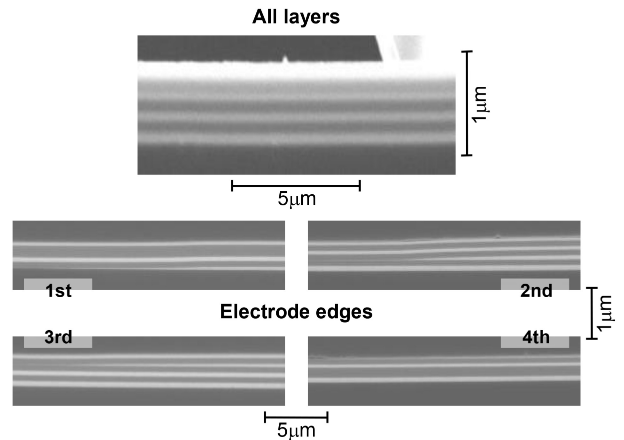

(c) CP-SEM photograph.

FIGURE 1. Multilayer crossbar array of amorphous metal-oxide semiconductor thin films.

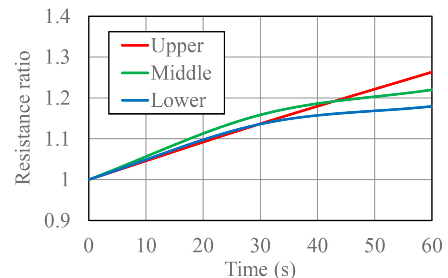

FIGURE 2. Resistance change over time by voltage application.

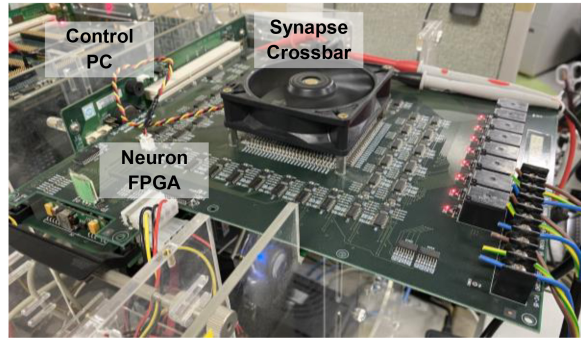

(a) Overview photograph.

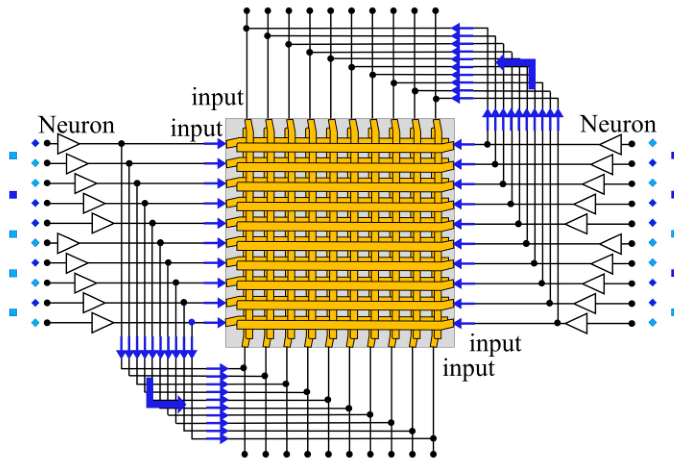

(b) Training phase.

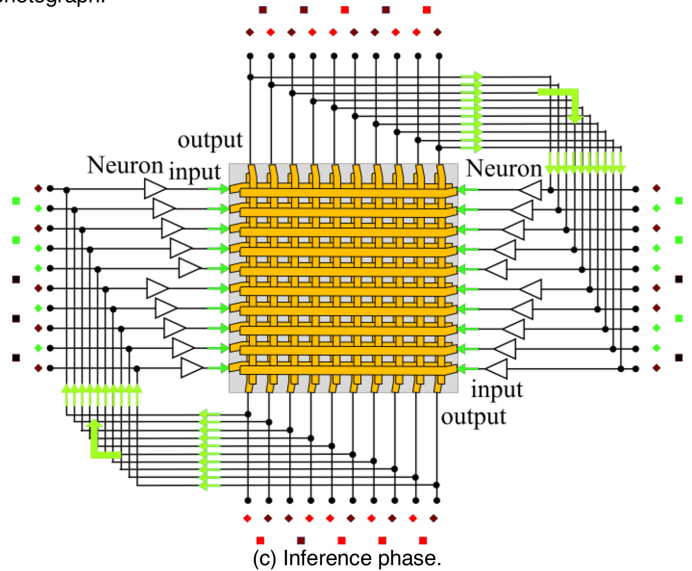

(c) Inference phase.

FIGURE 3. Implementation into a neuromorphic system.

is completed, where each of the three conductance change layers is sandwiched between the electrodes, the first and third electrodes constitute the vertical electrodes of 20 lines, and the second and fourth electrodes constitute the horizontal electrodes of 20 lines, and it can be said $10 \times 10 \times 3 = 300$ crosspoint-type devices using AOS conductance change layers are integrated in three-dimensional structure. The cross- section-polisher scanning-electron-microscope (CP-SEM) photograph is shown in Fig. 1(c). It should be noted that the first and third electrodes are staggeredly located, and the second and fourth electrodes are also the same, as shown in Fig. 1(b). In addition, they are patterned through a metal mask, and the electrode edges are gently sloping, as shown in Fig. 1(c). As consequence, there is no coverage problem. If they should be patterned by photolithography, some revision would be needed.

The resistance change over time by voltage application is shown in Fig. 2. A voltage of 3 V is applied, currents are measured, the resistance is obtained, and its ratios to the initial values are plotted. It is found that the resistance increases with time. The mechanism of the resistance increases is speculated as follows [29]. The first candidate is the decrease in oxygen vacancies due to the uptake of oxygen atoms. The oxygen atoms in the IGZO lattice or from outside the IGZO thin film move to the oxygen vacancies and annihilate them, the oxygen vacancies that act as donors decrease, and free electrons decrease. The second candidate is the increase in trap states due to impact of the free carriers in the AOS conductance change layer. The free electrons are accelerated and collide to the IGZO lattice, trap states are generated and capture free electrons, and free electrons decrease and are simultaneously scattered by them. In any case, the resistance changes can be regarded as an analog memristive characteristic and utilized for the modified Hebbian learning [39], [41].

III. IMPLEMENTATION INTO A NEUROMORPHIC SYSTEM

The implementation into a neuromorphic system is shown in Fig. 3. The overview photograph is shown in Fig. 3(a). Neuron elements are formed externally in an FPGA board and connected to the multilayer crossbar array of AOS thin films as synapse elements, which are controlled by a personal computer.

The training phase is shown in Fig. 3(b). Here, the blue arrows indicate the directions of signals, blue bright and dark squares indicate on and off input signals, and blue

bright and dark rhombuses indicate positive and negative input voltages. During the training phase, either high training voltages of ±3 V or no voltage is applied between the horizontal and vertical electrodes, so that the conductance change is induced in the conductance change layers, which is the modified Hebbian learning. Namely, the blue bright and dark rhombuses indicate +1.5 V and −1.5 V, respectively. If the voltage of either ±3 V is applied to the crosspoint-type device, the conductance change is induced, and otherwise, it is not induced. It should be noted that the training voltages themselves and their inverted voltages are applied to the neighboring electrode pairs, by which bias in the sign of the voltage can be avoided.

The inference phase is shown in Fig. 3(c). Here, the green arrows indicate the directions of signals, green bright and dark squares indicate on and off input signals, green bright and dark rhombuses indicate positive and negative input voltages, red bright and dark rhombuses indicate positive and negative output voltages, and red bright and dark squares indicate on and off output signals. During the inference phase, low input voltages of ±0.1 V are applied to only the horizontal electrodes, so that the resistance change is not induced. Namely, the green bright and dark rhombuses indicate +0.1 V and −0.1 V, respectively. After currents flow through the circuit built by the crosspoint-type devices, the voltages are determined at all nodes. Some output voltages are measured from the vertical electrodes, and they are distinguished as either on or off signals depending on whether they are positive or negative in the corresponding neighboring electrodes pairs. Namely, the red bright and dark rhombuses indicate some positive and negative voltages, respectively. If one output voltage is positive and the other neighboring voltage is negative, they are distinguished as on signals, and vice-versa, they are distinguished as off signals. Because the input voltage is low, the output voltage is also low, but it is easily possible to check only the sign. It should be noted that the output voltages are feedbacked to the input voltages until the steady state after dynamic behavior of the neuromorphic system. This is because the initial output voltage may be altered after they are feedbacked, and the final output voltage is supposed to fall into the minimum energy state of this system, that is, the trained voltage pattern during the training phase.

IV. ASSOCIATIVE MEMORY FUNCTION

The associative memory function is shown in Fig. 4. The algorithm is shown in Fig. 4(a). During the training phase, alphabet characters of "**T**" and "**L**" are learned. First, a two-dimensional pixel pattern of 3×3 pixels of "**T**" is transformed to a one-dimensional signal pattern of 9 components, and the signal pattern is inputted to the neuromorphic system, namely, the corresponding voltages and inverted voltages of 18 pieces are applied to the horizontal and vertical electrodes for 1 second. Next, a signal pattern of "**L**" is similarly inputted in sequence. During the inference phase, alphabet characters of "**T**" and "**L**" are reproduced. First, a slightly distorted pixel pattern, namely, a one-pixel flipped pattern of 3×3 pixels of "**T**", is transformed to a signal pattern of 9 components, the signal pattern is inputted to the neuromorphic system, namely, the corresponding voltages and inverted voltages of 18 pieces are applied to the horizontal electrodes for 1 second, some signal pattern is outputted, namely, the corresponding voltages and inverted voltages of 18 pieces are measured from the vertical electrodes, the one-dimensional signal pattern of 9 components is transformed to the two-dimensional pixel pattern of 3×3 pixels, and the outputted pixel pattern is compared with the alphabet characters of "**T**". Subsequently, these procedures are repeated also for different distorted pixel patterns. Next, slightly distorted signal patterns of "**L**" are inputted, and the outputted pixel pattern is compared with the alphabet characters of "**L**". Then, these procedures are reiterated many times.

The experimental results are shown in Fig. 4(b). It is confirmed that the alphabet characters of "**T**" and "**L**" are successfully learned, namely, the alphabet characters of "**T**" and "**L**" are successfully reproduced, except for one failure example, which may be due to the unwanted deviation of the analog memristive characteristic of the multilayer crossbar array of AOS thin films. In any case, it can be said that an associative memory function is confirmed. It should be noted that the associative memory function is confirmed in practical time, although the resistance change is slow, as shown in Fig. 2. This is because output voltages are determined by majority vote of the crosspoint-type device, where even the small differences in the resistance values are meaningful. Moreover, it is expedient, because multiple overrides of various trainings become possible.

The comparison of resistance change between theory and experiment is shown in Fig. 5. The voltage application combination is shown in Fig. 5(a). During the training phase, voltage is applied or not for each crosspoint-type device for each "**T**" and "**L**", and therefore there are three voltage application combinations: Combination 1, where no voltage is applied and the conductance change is not induced; Combination 2, where voltage is applied in only one case; and Combination 3, where voltage is applied in both cases. Therefore, the resistance difference between Combination 1 and Combinations 2 and 3 corresponds to the conductance change during the training phase.

The experimental results are shown in Fig. 5(b). The resistance is measured for all the crosspoint-type devices using AOS conductance change layers after the training and inference are successfully done, and its values are plotted for each voltage application combination. The resistance values for the crosspoint-type devices where the alphabet characters are successfully reproduced are plotted with the standard deviations in the figure above. It is found that the resistance value increases as the number of voltage application case increases, which is as expected. It should be noted that the alphabet characters are successfully reproduced, although the resistance change is small and the standard deviations

(a) Algorithm.

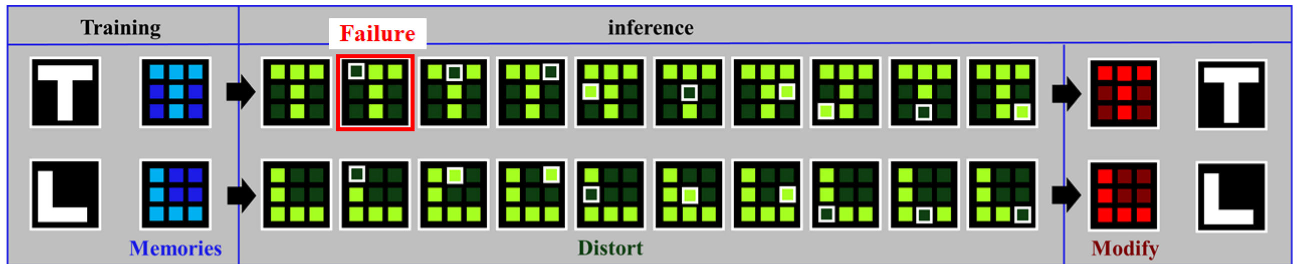

(b) Experimental results.

FIGURE 4. Associative memory function.

a quite large, which is covered because the inference is done by a majority vote of many crosspoint-type devices. Moreover, the resistance values for the one failure example shown in Fig. 4(b) is also plotted in the figure below. The relationship of the resistance values between the voltage application combination is not as expected, namely, the resistance value for Combination 2 must be less than but is actually more than that for Combination 3, which clarifies that the failure example is due to the unwanted deviation of the analog memristive characteristic. Therefore, this problem will be solved by improving the characteristic uniformity of the crosspoint-type devices.

The power consumption can be considered as follows. Because the resistance value is several kΩ as shown in Fig. 5(b), the power consumption per crosspoint-type device is several mW when a voltage of ±3 V is applied during the training phase and several μW when a voltage of ±0.1 V is applied during the inference phase, respectively. Because the size is 1.2 × 1.2 mm, the power consumption per area in the crosspoint-type device is several mW/mm^2 during the training phase and several $\mu W/mm^2$ during the inference phase, respectively. Although the size is currently large, if the crosspoint-type device is miniaturized down to, for example, 100 × 100 nm, the power consumption per crosspoint-type device is several tens pW during the training phase and several tens fW during the inference phase, respectively. Even if 100 trillion synapses, which is the same number as in a human brain, are integrated, the power consumption will be several W at most, which is less value than in a human brain.

		T	
		No application	Application
L	No application	1	2
	Application	2	3

(a) Voltage application combinations.

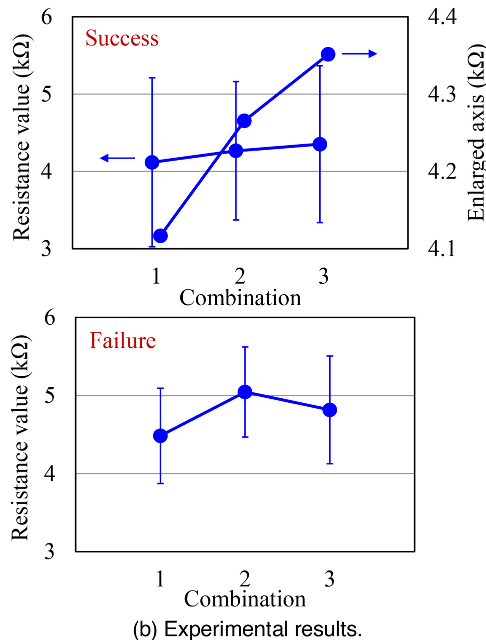

(b) Experimental results.

FIGURE 5. Comparison of resistance change between theory and experiment.

V. CONCLUSION

A multilayer crossbar array has been developed using AOS thin films and implemented into a neuromorphic system. The multilayer structure can be realized as three-dimensional structure, because the AOS thin films can be deposited by a simple sputtering method without heat treatment, which does not damage the underlying already deposited structures. First, Au thin films were deposited by vapor evaporation as electrodes, an α-IGZO thin film was deposited by a RF magnetron sputtering method as a conductance change layer, and these processes were repeated. A multilayer crossbar array was completed, where each of the three conductance change layers was sandwiched between the electrodes, and a lot of crosspoint-type devices using AOS conductance change layers were integrated in three-dimensional structure. Next, the multilayer crossbar array was implemented into a neuromorphic system with modified Hebbian learning, which enables autonomous learning without control circuitry. Alphabet characters were learned during the training phase, and they were reproduced during the inference phase. It can be said that an associative memory function was confirmed, and the comparison between theory and experiment was also verified, which guarantees the possibility of further advanced functions. These results lead to astronomical LSI of synaptic elements in neuromorphic systems in the future.

REFERENCES

[1] J. McCarthy, M. L. Minsky, N. Rochester, and C. E. Shannon, "A proposal for the Dartmouth summer research project on artificial intelligence," in *Dartmouth Conf.*, 1956.

[2] P. H. Winston, *Artificial Intelligence*. Reading, MA, USA: Addison-Wesley Longman Publ., 1992.

[3] S. Russell and P. Norvig, *Artificial Intelligence: A Modern Approach*. Upper Saddle River, NJ, USA: Prentice-Hall, 2009.

[4] W. S. McCulloch, and W. Pitts, "A logical calculus of the ideas immanent in nervous activity," *Bull. Math. Biophys.*, vol. 5, pp. 115–133, Dec. 1943.

[5] P. D. Wasserman, *Neural Computing: Theory and Practice*. New York, NY, USA: Coriolis Group, 1989.

[6] J. E. Dayhoff, *Neural Network Architectures: An Introduction*. New York, NY, USA: Van Nostrand Reinhold, 1990.

[7] D. Ferrucci *et al.*, "Building Watson: An overview of the DeepQA project," *AI Mag.*, vol. 31, no. 3, pp. 59–79, 2010.

[8] C. C. Aggarwal, *Neural Networks and Deep Learning: A Textbook*. Cham, Switzerland: Springer, 2018.

[9] C. Mead, *Analog VLSI and Neural Systems*. Reading, MA, USA: Addison-Wesley, 1989.

[10] J. Hsu, "IBM's new brain," *IEEE Spectr.*, vol. 51, no. 10, pp. 17–19, Oct. 2014.

[11] P. A. Merolla *et al.*, "A million spiking-neuron integrated circuit with a scalable communication network and interface," *Science*, vol. 345, pp. 668–673, Aug. 2014.

[12] S. Furber, "Large-scale neuromorphic computing systems," *J. Neural Eng.*, vol. 13, Aug. 2016, Art. no. 51001.

[13] M. Prezioso, F. Merrikh-Bayat, B. D. Hoskins, G. C. Adam, K. K. Likharev, and D. B. Strukov, "Training and operation of an integrated neuromorphic network based on metal-oxide memristors," *Nature*, vol. 521, pp. 61–64, May 2015.

[14] X. Zhang, A. Huang, Q. Hu, Z. Xiao, and P. K. Chu, "Neuromorphic computing with memristor crossbar," *Physica Status Solidi A*, vol. 215, Jul. 2018, Art. no. 1700875.

[15] K. Nomura, H. Ohta, A. Takagi, T. Kamiya, M. Hirano, and H. Hosono, "Room-temperature fabrication of transparent flexible thin-film transistors using amorphous oxide semiconductors," *Nature*, vol. 432, pp. 488–492, Nov. 2004.

[16] M. Kimura, "Emerging applications using metal-oxide semiconductor thin-film devices," *Jpn. J. Appl. Phys.*, vol. 58, May 2019, Art. no. 90503.

[17] E. Tokumitsu, M. Senoo, and T. Miyasako, "Use of ferroelectric gate insulator for thin film transistors with ITO channel," *Microelectron. Eng.*, vol. 80, pp. 305–308, Jun. 2005.

[18] H. Yin *et al.*, "Fully transparent nonvolatile memory employing amorphous oxides as charge trap and transistor's channel layer," *Appl. Phys. Lett.*, vol. 93, Oct. 2008, Art. no. 172109.

[19] T.-C. Huang and K.-T. Cheng, "Design for low power and reliable flexible electronics: Self-tunable cell-library design," *J. Display Technol.*, vol. 5, no. 6, pp. 206–215, Jun. 2009.

[20] K. Kaneko, N. Inoue, S. Saito, N. Furutake, and Y. Hayashi, "A novel BEOL transistor (BETr) with InGaZnO embedded in Cu-interconnects for on-chip high voltage I/Os in standard CMOS LSIs," in *VLSI-Technol. Dig. Tech.* 2011, pp. 120–121.

[21] S. Yamazaki, J. Koyama, Y. Yamamoto, and K. Okamoto, "15.1: Research, development, and application of crystalline oxide semiconductor," *Soc. Inf. Display*, vol. 43, no. 1, pp. 183–186, 2012.

[22] Y. Fujimoto, M. Uenuma, Y. Ishikawa, and Y. Uraoka, "Analysis of thermoelectric properties of amorphous InGaZnO thin film by controlling carrier concentration," *AIP Adv.*, vol. 5, Sep. 2015, Art. no. 97209.

[23] T. Matsuda, K. Umeda, Y. Kato, D. Nishimoto, M. Furuta, and M. Kimura, "Rare-metal-free high-performance Ga-Sn-O thin film transistor," *Sci. Rep.*, vol. 7, Mar. 2017, Art. no. 44326.

[24] K. Takechi *et al.*, "Demonstration of detecting small pH changes using high-sensitivity amorphous $InGaZnO_4$ thin-film transistor pH sensor system," *IEEE Trans. Electron Devices*, vol. 64, no. 2, pp. 638–641, Feb. 2017.

[25] K. Aoki *et al.*, "Magnetoresistive effect of amorphous In-Ga-Zn-O magnetic field sensors," *IEEE Electron Device Lett.*, vol. 38, no. 8, pp. 1143–1145, Aug. 2017.

[26] T. Matsuda, M. Uenuma, and M. Kimura, “Thermoelectric effect of amorphous Ga–Sn–O thin film,” *Jpn. J. Appl. Phys.*, vol. 56, Jun. 2017, Art. no. 70309.

[27] Y. Magari *et al.*, “Record-high-performance hydrogenated In–Ga–Zn–O flexible schottky diodes,” *ACS Appl. Mater. Interfaces*, vol. 12, pp. 47739–47746, Oct. 2020.

[28] Z. Q. Wang, H. Y. Xu, X. H. Li, H. Yu, Y. C. Liu, and X. J. Zhu, “Synaptic learning and memory functions achieved using oxygen ion migration/diffusion in an amorphous InGaZnO memristor,” *Adv. Funct. Mater.*, vol. 22, pp. 2759–2765, Jul. 2012.

[29] M. Kimura, Y. Koga, H. Nakanishi, T. Matsuda, T. Kameda, and Y. Nakashima, “In–Ga–Zn–O thin-film devices as synapse elements in a neural network,” *IEEE J. Electron Devices Soc.*, vol. 6, pp. 100–105, 2017.

[30] S. Sugisaki *et al.*, “Memristive characteristic of an amorphous Ga-Sn-O thin-film device,” *Sci. Rep.*, vol. 9, p. 2757, Feb. 2019.

[31] A. Kurasaki *et al.*, “Memristive characteristic of an amorphous Ga-Sn-O thin-film device with double layers of different oxygen density,” *Materials*, vol. 12, p. 3236, Oct. 2019.

[32] X. Liang, Z. Li, L. Liu, S. Chen, X. Wang, and Y. Pei, “Artificial synaptic transistor with solution processed InO_x channel and AlO_x solid electrolyte gate,” *Appl. Phys. Lett.*, vol. 116, Jan. 2020, Art. no. 12102.

[33] M. Pereira *et al.*, “Noble-metal-free memristive devices based on IGZO for neuromorphic applications,” *Adv. Electron. Mater.*, vol. 6, Oct. 2020, Art. no. 2000242.

[34] Y. Takishita *et al.*, “Memristor property of an amorphous Sn-Ga-O thin-film device deposited using mist chemical-vapor-deposition method,” *AIP Adv.*, vol. 10, Mar. 2020, Art. no. 35112.

[35] S. Song *et al.*, “Solution-processed oxide semiconductor-based artificial optoelectronic synapse array for spatiotemporal synaptic integration,” *J. Alloys Comp.*, vol. 857, Mar. 2021, Art. no. 158027.

[36] Y. Shibayama, Y. Ohnishi, T. Katagiri, Y. Yamamoto, Y. Nakashima, and M. Kimura, “Amorphous-metal-oxide-semiconductor thin-film planar-type spike-timing- dependent-plasticity synapse device,” *IEEE Electron Device Lett.*, vol. 42, no. 7, pp. 1014–1016, Jul. 2021.

[37] L. Hu, J. Yang, J. Wang, P. Cheng, L. O. Chua, and F. Zhuge, “All-optically controlled memristor for optoelectronic neuromorphic computing,” *Adv. Funct. Mater.*, vol. 31, Jan. 2021, Art. no. 2005582.

[38] Y. Ohnishi, Y. Shibayama, T. Katagiri, K. Morigaki, K. Yachida, and M. Kimura, “Amorphous Ga–Sn–O thin-film crosspoint-type spike-timing-dependent-plasticity device,” *Jpn. J. Appl. Phys.*, vol. 60, Jul. 2021, Art. no. 78003.

[39] M. Kimura, R. Sumida, A. Kurasaki, T. Imai, Y. Takishita, and Y. Nakashima, “Amorphous metal oxide semiconductor thin film, analog memristor, and autonomous local learning for neuromorphic systems,” *Sci. Rep.*, vol. 11, p. 590, Jan. 2021.

[40] K. Nomura *et al.*, “Three-dimensionally stacked flexible integrated circuit: Amorphous oxide/polymer hybrid complementary inverter using n-type a-In-Ga-Zn-O and *p*-type poly-(9, 9-dioctylfluorene-co-bithiophene) thin-film transistors,” *Appl. Phys. Lett.*, vol. 96, Jun. 2010, Art. no. 263509.

[41] M. Kimura, R. Morita, S. Sugisaki, T. Matsuda, T. Kameda, and Y. Nakashima, “Cellular neural network formed by simplified processing elements composed of thin-film transistors,” *Neurocomputing*, vol. 248, pp. 112–119, Jul. 2017.